Journal of Non-Newtonian Fluid Mechanics 349 (2026) 105600

Contents lists available at ScienceDirect

Journal of Non-Newtonian Fluid Mechanics

journal homepage: www.elsevier.com/locate/jnnfm

Full length article

Effect of the long-range van der Waals forces on the motion of an elongated bubble through a shear-thinning fluid

Davide Picchi [a,*], Mohamed Berkani [b], Gianluca Lavalle [b], Pietro Poesio [a]

[a] Department of Mechanical and Industrial Engineering, University of Brescia, Brescia 25123, Italy
[b] Mines Saint-Etienne, Univ. Lyon, CNRS, UMR 5307 LGF, Centre SPIN, F-42023 Saint-Etienne, France

ARTICLE INFO

Keywords:
Elongated bubble
Thin film
Disjoining pressure
Shear-thinning fluid
Film thickness

ABSTRACT

We study the influence of the long-range van der Waals forces on the motion of an elongated bubble in a capillary tube filled with a non-Newtonian shear-thinning fluid. Using the lubrication theory we extend the classical Bretherton thin film model to include the Lifshitz form of the disjoining pressure in the context of shear-thinning fluids to investigate how much it impacts on the bubble characteristics in both planar and circular geometries. The fluid rheology is described by the Ellis viscosity model so that both the low-shear-rate Newtonian viscosity and the shear-thinning effects are properly described. Interestingly, the stabilizing effect of the disjoining pressure change the shape of the elongated bubble suppressing the undulations at the rear of the elongated bubble. In addition, thanks to a proper rescaling of the effective viscosity, we propose a generalization of the scaling law for the dimensionless film thickness that applies to both Newtonian and shear-thinning fluids. Such scaling law captures the ultra-low capillary number regime (dominated by the disjoining pressure) where the film thickness assumes a constant value and the low capillary number regime (dominated by surface tension) where the film thickness follows the classical 2/3 scaling law typical of thin-film problems. We also explore the limiting case of a power-law fluid.

1. Introduction

Elongated bubbles moving in confined environments are common in many fields including microfluidics [e.g., 1–4], medicine [e.g., 5–8], and subsurface flows. Typically, when inertia and gravity are negligible, viscous forces compete only with surface tension and the bubble assumes a bullet shape, also known as Bretherton bubble or Taylor bubble acknowledging the seminal works of Taylor [9] and Bretherton [10]. In this context, elongated bubbles have been extensively studied, starting with early experiments that correlate the speed of the bubble with the capillary number [9,11], and pursuing with the development of film model based on the lubrication theory proposed by Bretherton [10]. Later, researchers have proposed many extensions to incorporate the effect of viscous forces, inertia, and variable surface tension [just to mention a short list, see 12–17].

Although most of the working fluids, such as polymer solutions, emulsions, and biological fluids have a complex rheology and they typically behave like non-Newtonian shear-thinning fluids, the impact of the fluid rheology on the motion of an elongated bubble is still an object of research. The first attempts primarily focused on extending the scaling laws valid in the Newtonian scenario to power-law fluids [18–24] ignoring that the power-law model fails to describe the zero- and infinity-shear rate behavior [25] leading to nonphysical results in describing the velocity field [see e.g., 26–31]. To fix such inconsistencies, Hewson et al. [32] developed a model based on the lubrication approximation assuming that the shear-thinning fluid follows the Ellis viscosity model [33] while Moreira et al. [34] and Sontti and Atta [35] perform numerical simulations using the Carreau–Yasuda [36,37] viscosity model. More recently, Picchi et al. [38] proposed a generalization of the Bretherton film equations to shear-thinning fluids showing that the film thickness follows the classical two-third scaling laws typical of many thin-film problems [39] also in the case of shear-thinning fluids. Such scaling laws are recovered introducing a generalized capillary number that embeds both the zero-shear-rate and the shear-thinning effects. This has been confirmed both experimentally and numerically [40,41] and holds not only in low capillary number regimes (i.e., the Bretherton theory is applicable for capillary numbers of the order of $\mathcal{O}(10^{-3})$ – $\mathcal{O}(10^{-2})$) but also in regimes where viscous effects compete with surface tension at finite capillary numbers.

Unfortunately, the aforementioned theory is not applicable when the film surrounding the elongated bubble is so thin that a proper description of the underlying physics requires to account for long-range van der Waals intermolecular forces [42,43]. This regime manifests

* Corresponding author.
E-mail address: davide.picchi@unibs.it (D. Picchi).

https://doi.org/10.1016/j.jnnfm.2026.105600
Received 23 December 2025; Received in revised form 8 April 2026; Accepted 11 April 2026
Available online 20 April 2026

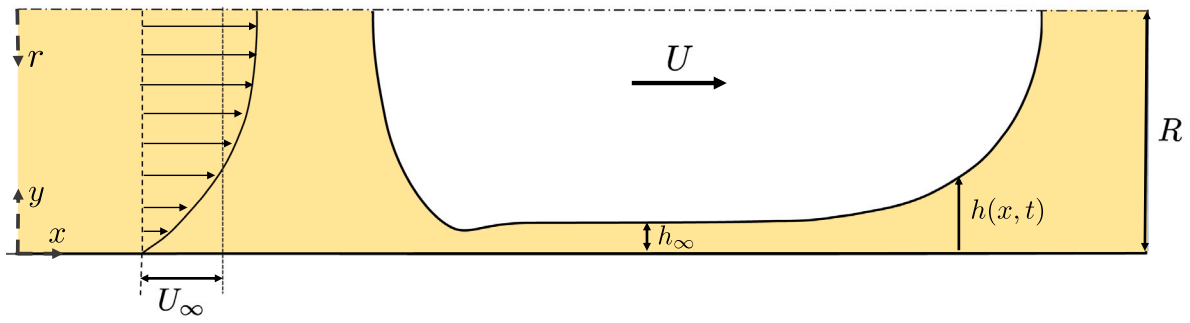

Fig. 1. Sketch of the elongated bubble flowing at constant speed U in a tube of half-width R. The motion of the bubble is driven by an imposed volume flux of averaged speed U_∞.

when the capillary number is ultra-low and the interfacial length scale approaches the molecular dimensions, requiring a proper correction of the normal stress boundary condition in the thin film in the form of the disjoining pressure [44–46]. So far, attention has been given primarily to account for the classical Lifshitz form of the disjoining pressure on Newtonian films [see e.g., 47–50], showing the breakdown of the two-third scaling law in regimes dominated by van der Waals forces. The impact of such molecular effects on the bubble characteristics in the case of non-Newtonian fluids is still an open question.

To fill this gap, our goal is to investigate the competition between the rheology, namely an inelastic shear thinning fluid, and the film dynamics in regimes dominated by the disjoining pressure. We will focus on regimes where inertia and gravitational effects can be neglected and the motion of the elongated bubble is driven by a fixed volumetric flux far behind the bubble. The main idea is to generalize the Bretherton theory valid for shear thinning fluids proposed by Picchi et al. [38] to include long-range van der Waals forces and to understand whether the two-third scaling law for the film thickness breaks down at ultra low capillary numbers. To do so, we use the classical lubrication theory to describe the flow of an Ellis fluid in the meniscus accounting for the Lifshitz form of the disjoining pressure (Section 2). Then, by matching the solution in the thin film to the spherical cap we derive a generalized scaling law for the film thickness (Section 3.2). Our theory holds only when the capillary number is small and applies to both planar and axisymmetric geometry. The main result will be to show that a proper rescaling of the effective viscosity allows to find a master curve that holds for both Newtonian and inelastic shear-thinning fluids in regimes dominated by the disjoining pressure and not. In other words we aim at unifying the description of the dynamics of elongated bubbles in a range of low and ultra-low capillary numbers. In Appendix C we also show the limiting case of a power-law fluid.

2. Theoretical derivation

2.1. Governing equations

We consider an inviscid elongated bubble moving at constant speed U in a capillary tube of half-width R filled with a shear-thinning fluid whose viscosity is described by the Ellis viscosity model [25,33,51]. The motion is driven by an imposed volumetric flux far behind the bubble with average speed U_∞ in regimes where inertia and gravity can be neglected and the bubble is symmetrical with respect to the tube axis. We assume that the thin film region surrounding the bubble is in the visco-capillary regime, namely that the viscous effects balances with surface tension, so that it can be treated using the lubrication approximation typical of the Landau–Levich–Derjaguin–Bretherton problems [see 39,42,52,53]. Specifically, the elongated bubble is sufficiently long that there exist a region where the film thickness is almost flat and equal to h_∞ in Fig. 1 and the menisci in the front and the rear could be treated separately. Far form the uniform film, instead, the shape of the meniscus is dominated by surface tension resulting in a spherical cap either in the front and the rear of the bubble.

The main idea is to consider a very thin film, i.e., $h_\infty \ll R$, and to zoom into the film region by normalizing the transverse spatial coordinate by the uniform film thickness h_∞ and to scale the axial coordinate by the factor h_∞/ε where $\varepsilon \ll 1$ is the scale parameter (that will be defined later on) giving

$$\tilde{x} = \frac{x}{h_\infty/\varepsilon} \qquad \tilde{y} = \frac{y}{h_\infty}\,. \tag{1}$$

Similarity to Bretherton [10], since the film is much thinner than the tube half-width, $h_\infty/R \ll 1$, the planar and the axisymmetric description are equivalent as can be easily seen by the following relations on spatial derivatives

$$\frac{1}{r}\frac{\partial}{\partial r}(r\star) = \frac{1}{R}\left(-\frac{R}{h_\infty}\frac{\partial \star}{\partial \tilde{y}} + \frac{\star}{1-\tilde{y}(h_\infty/R)}\right) \approx -\frac{\partial \star}{\partial y}, \tag{2a}$$

$$\frac{1}{r}\frac{\partial}{\partial r}\left(r\frac{\partial \star}{\partial r}\right) = \frac{1}{h_\infty R}\left(\frac{R}{h_\infty}\frac{\partial^2 \star}{\partial \tilde{y}^2} - \frac{1}{1-\tilde{y}(h_\infty/R)}\frac{\partial \star}{\partial \tilde{y}}\right) \approx \frac{\partial^2 \star}{\partial y^2}. \tag{2b}$$

where $r = R - y$. Thus, the derivation is made in terms of planar coordinates and the geometrical effect will enter only in the mass balance between the film and the flow far ahead.

The lubrication approximation holds when the film is shallow, namely $|dh/dx| \ll 1$, with $h(x,t)$ denoting the location of the interface. Using the bubble velocity U as the reference scale for the velocity in the axial direction, εU as the reference for the velocity in the transverse direction, the capillary pressure scaling $\sigma\varepsilon^2/h_\infty$ as the reference scale for pressure, the governing equation of the liquid in the film region yields

$$\frac{\partial \tilde{u}}{\partial \tilde{x}} + \frac{\partial \tilde{v}}{\partial \tilde{y}} = 0\,, \tag{3}$$

$$\varepsilon\, Re\left[\frac{\partial \tilde{u}}{\partial \tilde{t}} + \tilde{u}\frac{\partial \tilde{u}}{\partial \tilde{x}} + \tilde{v}\frac{\partial \tilde{u}}{\partial \tilde{y}}\right] = -\frac{\varepsilon^3}{\mathrm{Ca}}\frac{\partial \tilde{p}}{\partial \tilde{x}} + 2\varepsilon^2\frac{\partial}{\partial \tilde{x}}\left[\tilde{\mu}\frac{\partial \tilde{u}}{\partial \tilde{x}}\right] + \frac{\partial}{\partial \tilde{y}}\left[\tilde{\mu}\left(\frac{\partial \tilde{u}}{\partial \tilde{y}} + \varepsilon^2\frac{\partial \tilde{v}}{\partial \tilde{x}}\right)\right], \tag{4}$$

$$\varepsilon^3\, Re\left[\frac{\partial \tilde{v}}{\partial \tilde{t}} + \tilde{u}\frac{\partial \tilde{v}}{\partial \tilde{x}} + \tilde{v}\frac{\partial \tilde{v}}{\partial \tilde{y}}\right] = -\frac{\varepsilon^3}{\mathrm{Ca}}\frac{\partial \tilde{p}}{\partial \tilde{y}} + 2\varepsilon^2\frac{\partial}{\partial \tilde{y}}\left[\tilde{\mu}\frac{\partial \tilde{v}}{\partial \tilde{y}}\right] + \varepsilon^2\frac{\partial}{\partial \tilde{x}}\left[\tilde{\mu}\left(\frac{\partial \tilde{u}}{\partial \tilde{y}} + \varepsilon^2\frac{\partial \tilde{v}}{\partial \tilde{x}}\right)\right], \tag{5}$$

where

$$\tilde{\mu} = \frac{\mu}{\mu_0} = \frac{1}{1+(\tilde{\tau}/El)^{\alpha-1}}\,, \tag{6}$$

is the Ellis viscosity normalized by the zero-shear-rate viscosity expressed as a function of the magnitude of the shear-stress tensor

$$\tilde{\tau} = \sqrt{\left[\tilde{\mu}\left(\frac{\partial \tilde{u}}{\partial \tilde{y}} + \varepsilon^2\frac{\partial \tilde{v}}{\partial \tilde{x}}\right)\right]^2 + 2\varepsilon^2\left(\tilde{\mu}\frac{\partial \tilde{u}}{\partial \tilde{x}}\right)^2 + 2\varepsilon^2\left(\tilde{\mu}\frac{\partial \tilde{v}}{\partial \tilde{y}}\right)^2}\,, \tag{7}$$

while the four dimensionless parameters of the problem are the shear-thinning index α, the Ellis, the Reynolds, and the capillary numbers given by

$$El = \frac{\tau_{1/2} h_\infty}{U \mu_0} \qquad Re = \frac{\rho U h_\infty}{\mu_0} \qquad Ca = \frac{\mu_0 U}{\sigma} . \tag{8}$$

In the definition of the Ellis number, μ_0 is the zero-shear-rate viscosity, namely the Newtonian viscosity at small shear-rates; α determines the degree of shear-thinning; $\tau_{1/2}$ is a rheological parameter that controls the onset of the shear thinning effect and it is defined as the shear-stress at which the effective viscosity is half of the zero-shear-rate viscosity. From the practical point of view, the Ellis viscosity model is applicable to many polymer solutions (e.g., CMC and xanthane solutions) where the rheological constants are typically in the range $\alpha \in (1,4)$ and $\tau_{1/2} = \mathcal{O}(10^{-3} \div 10)$ Pa, see Bird et al. [25]. Thus, the Ellis number controls the onset of the shear thinning effect: when $El \to \infty$ the fluid is Newtonian $\tilde{\mu} \to 1$, while for $El \to 0$ the shear-thinning effect dominates over the zero-shear-rate effect and the fluid approaches the power-law behavior with effective viscosity $\mu \to \kappa \dot{\gamma}^{1/\alpha - 1}$ with $\kappa = \mu_0^{1/\alpha} \tau_{1/2}^{(1-1/\alpha)}$.

The governing equations are subjected to the no-slip (and no penetration) boundary condition at the wall, free-surface boundary condition at the fluid–bubble interface, while the boundary condition for normal stresses accounting for the effect of the disjoining pressure on a non uniform film thickness [see 48,54] yields

$$-\tilde{p}|_\eta + 2Ca\,\varepsilon^{-1}\,\tilde{\mu}\,\frac{\partial \tilde{v}}{\partial \tilde{y}}\bigg|_\eta = \frac{\left.\frac{\partial^2 \eta}{\partial \tilde{x}^2}\right|_\eta}{\left[1 + \varepsilon^2 \left(\left.\frac{\partial \eta}{\partial \tilde{x}}\right|_\eta\right)^2\right]^{3/2}} + \frac{\beta}{\eta^3}\left[1 - \frac{3\varepsilon^2}{4}\left(\left(\frac{\partial \eta}{\partial \tilde{x}}\right)^2 - h\frac{\partial^2 \eta}{\partial \tilde{x}^2}\right)\right], \tag{9}$$

where $\eta = h(x,t)/h_\infty$ is the dimensionless film thickness and β is the van der Waals parameter defined in Hammoud et al. [50]:

$$\beta = \frac{A}{6\pi h_\infty^2 \sigma Ca^{\frac{2}{3}}} , \tag{10}$$

with A being the Hamaker constant, typically of the order of $10^{-20} - 10^{-19}$ J. If the Hamaker constant is positive $A > 0$ the intermolecular forces are repulsive and, then, stabilize the liquid film; instead, for $A < 0$ such forces are attractive and can destabilize the film leading to film rupture and dewetting. Compared to Picchi et al. [38], Eq. (9) is an extension of the normal stress condition to regimes where the film thickness is thin enough that long-range van der Waals forces become significant. In this work, we are interested only in regimes where the intermolecular forces are repulsive, $\beta > 0$, and, therefore, stabilize the liquid film; regimes where $\beta < 0$ are beyond the scope of this work (note that we have defined the sign of β with an opposite convention with respect to Hammoud et al. [50]).

2.2. The thin-film model

Following the derivation of the Landau–Levich–Derjaguin–Bretherton problems, the equation to describe the thin-film of the elongated bubble is obtained by taking the limit of $\varepsilon \ll 1$ and $\varepsilon Re \ll 1$ in Eqs. (4) and (5). These conditions are required to apply the lubrication approximation in the thin-film region, namely that inertial effects can be neglected and the scale parameter is chosen as $\varepsilon = Ca^{1/3} \ll 1$ in order to balance the viscous stress and the pressure gradient in the momentum balance in the axial direction (Eq. (4)); as a result, there is no pressure gradient in the transverse direction, $\partial \tilde{p}/\partial \tilde{y} = 0$. Therefore, the axial momentum yields, at the leading order in ε,

$$0 = -\frac{d\tilde{p}}{d\tilde{x}} + \frac{d}{d\tilde{y}}\left(\tilde{\mu}\frac{d\tilde{u}}{d\tilde{y}}\right) , \tag{11}$$

where the magnitude of the shear stress within the effective viscosity, Eq. (7), reduces to $\tilde{\tau} \approx |\tilde{\mu}\, d\tilde{u}/d\tilde{x}|$. In this limit, it follows from Eq. (9) that the pressure is given by the curvature of the interface and the Lifshitz form of the disjoining pressure [see 42,44]

$$\tilde{p} = -\frac{\partial^2 \eta}{\partial \tilde{x}^2} - \frac{\beta}{\eta^3} , \tag{12}$$

and, recalling that $\tilde{x} = x/(h_\infty Ca^{-1/3})$, the pressure gradient is given by

$$\frac{d\tilde{p}}{d\tilde{x}} = -\frac{d^3\eta}{d\tilde{x}^3} + 3\beta\frac{d\eta}{d\tilde{x}}\frac{1}{\eta^4} . \tag{13}$$

The velocity profile is obtained by integration of Eq. (11) subjected to the no slip condition at the solid wall and the free surface condition at the interface yielding

$$\tilde{u}(\tilde{y}) = \frac{1}{2}\frac{d\tilde{p}}{d\tilde{x}}\left(\tilde{y}^2 - 2\eta\tilde{y}\right) + \frac{1}{(\alpha+1)El^{\alpha-1}}\frac{d\tilde{p}}{d\tilde{x}}\left|\frac{d\tilde{p}}{d\tilde{x}}\right|^{\alpha-1}\left[(\eta - \tilde{y})^{\alpha+1} - \eta^{\alpha+1}\right] , \tag{14}$$

where the pressure gradient is given by Eq. (13). Then, we can write the mass balance between the uniform film and the transition regions in a reference frame moving with the bubble as

$$(0-U)h_\infty = \left(\frac{Q}{h} - U\right)h \qquad \text{or} \qquad \tilde{Q} = \eta - 1, \tag{15}$$

where the dimensionless flow rate is given by

$$\tilde{Q} = \frac{Q}{h_\infty U} = \int_0^\eta \tilde{u}(\tilde{y})\, d\tilde{y} = -\frac{1}{3}\frac{d\tilde{p}}{d\tilde{x}}\eta^3 - \frac{1}{(\alpha+2)El^{\alpha-1}}\frac{d\tilde{p}}{d\tilde{x}}\left|\frac{d\tilde{p}}{d\tilde{x}}\right|^{\alpha-1}\eta^{\alpha+2} . \tag{16}$$

From Eqs. (16) and (15) and recasting the axial variable accordingly to Bretherton [10] as $\xi = 3^{1/3}\tilde{x} = x/(h_\infty(3\mathrm{Ca})^{-1/3})$, we obtain the film model for the elongated bubble moving in a shear-thinning fluid that accounts for the disjoining pressure:

$$\frac{d^3\eta}{d\xi^3} - \frac{\tilde{\beta}}{\eta^4}\frac{d\eta}{d\xi} + \frac{3^\alpha}{(\alpha+2)El^{\alpha-1}}\left(\frac{d^3\eta}{d\xi^3} - \frac{\tilde{\beta}}{\eta^4}\frac{d\eta}{d\xi}\right)\left|-\frac{d^3\eta}{d\xi^3} + \frac{\tilde{\beta}}{\eta^4}\frac{d\eta}{d\xi}\right|^{\alpha-1}\eta^{\alpha-1} = \frac{\eta-1}{\eta^3} , \tag{17}$$

where $\tilde{\beta} = 3^{1/3}\beta$ is the rescaled van der Waals parameter

$$\tilde{\beta} = \frac{A}{2\pi h_\infty^2 \sigma (3Ca)^{\frac{2}{3}}} . \tag{18}$$

The film model shares the same structure as Picchi et al. [38], with the key difference that the pressure gradient here incorporates both capillary effects and long-range van der Waals forces as the driving mechanisms. The film thickness is a function of the axial coordinate, the Ellis number, the shear-thinning index, and the van der Waals parameter only, i.e., $\eta = \eta(\xi, El, \alpha, \tilde{\beta})$. As expected if $\tilde{\beta} \to 0$, we recover the same equation as Picchi et al. [38] and when both $\tilde{\beta} \to 0$ and $El \to \infty$, Eq. (17) simplifies into the work by Bretherton [10].

Although the power-law model is physically incorrect due the inconsistencies at low shear rates, we will show in Appendix C that, removing the first two terms from Eq. (17) in the limit of $El \to 0$, the proposed model reduces to the one for a power-law fluid.

2.3. Numerical solution of the film model

The film model, Eq. (17), is integrated numerically using the solver *ode15i* of Matlab starting from the uniform film region where $\eta \approx 1$ or, in dimensional coordinates $h(x,t) \approx h_\infty$. In order to find the boundary conditions necessary to start the integration in the direction of the front ($\xi \to \infty$) and the rear ($\xi \to -\infty$), Eq. (17) is linearized by expanding η as $\eta = 1 + \delta + \cdots$ with $\delta \ll 1$ obtaining

$$\frac{d^3\eta}{d\xi^3} - \tilde{\beta}\frac{d\eta}{d\xi} + \frac{3^\alpha}{(\alpha+2)El^{\alpha-1}}\left(\frac{d^3\eta}{d\xi^3} - \tilde{\beta}\frac{d\eta}{d\xi}\right)\left|-\frac{d^3\eta}{d\xi^3} + \tilde{\beta}\frac{d\eta}{d\xi}\right|^{\alpha-1} = \eta - 1 . \tag{19}$$

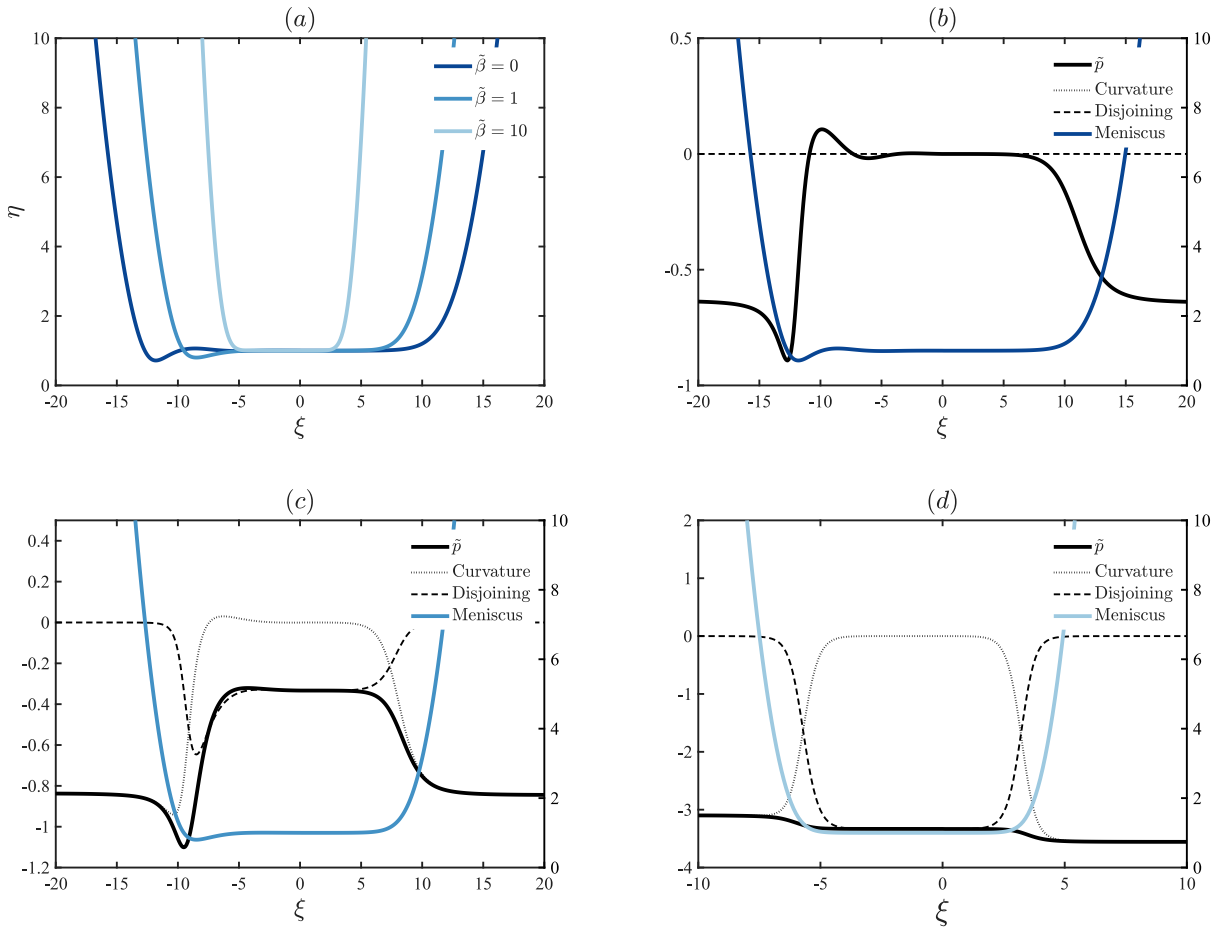

Fig. 2. (a) Effect of the van der Waals parameter on the shape of the meniscus in the Newtonian limit, $El \to \infty$ and $\alpha = 2$. The bubble have different length only due to choice of the integration constants. Evolution of the pressure and the contribution of the curvature ($-d^2\eta/d\xi^2$) and the disjoining pressure ($-\tilde{\beta}/\eta^3$) according to Eq. (12) in the Newtonian limit, $El \to \infty$ and $\alpha = 2$ for (b) left: contribution to the pressure for $\tilde{\beta} = 0$; right: bubble meniscus (c) $\tilde{\beta} = 1$; right: bubble meniscus (d) $\tilde{\beta} = 10$; right: bubble meniscus.

Since the third term on the left hand side that accounts for the shear-thinning effect is small (this will be justified *a posteriori* in Appendix B) we obtain an approximation that holds only near the uniform film

$$\frac{d^3\eta}{d\xi^3} - \tilde{\beta}\frac{d\eta}{d\xi} - \eta = -1 \qquad \text{when} \quad \eta \approx 1\,, \tag{20}$$

and it admits analytical solution of the form

$$\eta = 1 + Ae^{\lambda_1\xi} + Be^{\lambda_2\xi} + Ce^{\lambda_3\xi}\,, \tag{21}$$

where $\lambda_{1,2,3}$ are the roots of the characteristic equation $\lambda^3 - \tilde{\beta}\lambda - 1 = 0$ and A, B, and C are integration constants. Since in this work we are interested in regimes where the intermolecular forces are stabilizing, i.e., $\tilde{\beta} > 0$, the characteristic equation has one real and positive root, λ_1, and two complex conjugate roots, λ_2 and λ_3, for $0 \le \tilde{\beta} < (3/2^{\frac{2}{3}}) \approx 1.89$. Instead, for $\tilde{\beta} > 1.89$ the roots are all real with λ_1 positive and both λ_2 and λ_3 negative. This means that the shape of the meniscus changes depending on the van der Waals parameter and, in particular, it exhibits the undulations typical of the rear of the Bretherton's bubble only when $\tilde{\beta} < 1.89$; such undulations are suppressed by the stabilizing effect of the disjoining pressure.

For $\tilde{\beta} < 1.89$ Eq. (21) can be written as

$$\eta = 1 + Ae^{\lambda_1\xi} + \eta_0 \exp\left(\mathrm{Re}(\lambda_2)\xi\right) \cos\left[\mathrm{Im}(\lambda_2)\xi + \phi\right], \tag{22}$$

where $\eta_0 = \sqrt{B^2 + C^2}$ and $\phi = \arccos(B/\sqrt{B^2 + C^2})$ are two integration constants. Thus, the film model, Eq. (17), is integrated in the positive direction (to get the front profile) starting from

$$\eta \simeq 1 + Ae^{\lambda_1\xi}\,, \tag{23}$$

where the constant A (arbitrarily taken $A = 10^{-4}$) has the only effect of shifting the origin. To get the rear profile, we integrate in the negative direction starting from

$$\eta \simeq 1 + \eta_0 \exp\left[\mathrm{Re}(\lambda_2)\xi\right] \cos\left[\mathrm{Im}(\lambda_2)\xi + \phi\right], \tag{24}$$

where the constant η_0 has the only effect of moving the origin and it can be chosen arbitrarily; here, we set $\eta_0 = 10^{-3}$ to describe a sufficiently long uniform film region. In the rear, the harmonic part of the approximate solution is responsible for the undulation of the meniscus. The other constant ϕ is chosen via an iteration loop so that the curvature of the front (i.e., $d^2\eta/d\xi^2$ for $\xi \to \infty$) is equal to the curvature in the rear (i.e., $d^2\eta/d\xi^2$ for $\xi \to -\infty$) as typical of elongated bubbles at the low capillary number regime [10,38].

When $\tilde{\beta} > 1.89$, the approximated solution is given by Eq. (21) yielding an exponential meniscus in both the rear and the front menisci. In the front, the negative exponential functions corresponding to the second and the third roots can be neglected and the film model is integrated starting from Eq. (23) as in the previous case. In the rear, instead, the first exponential in Eq. (21) can be neglected and the expression can be re-casted in terms of hyperbolic functions as

$$\eta \simeq 1 + \exp\left(\frac{\lambda_2 + \lambda_3}{2}\xi\right)\left[(B + C)\cosh\left(\frac{\lambda_2 - \lambda_3}{2}\xi\right)\right.$$

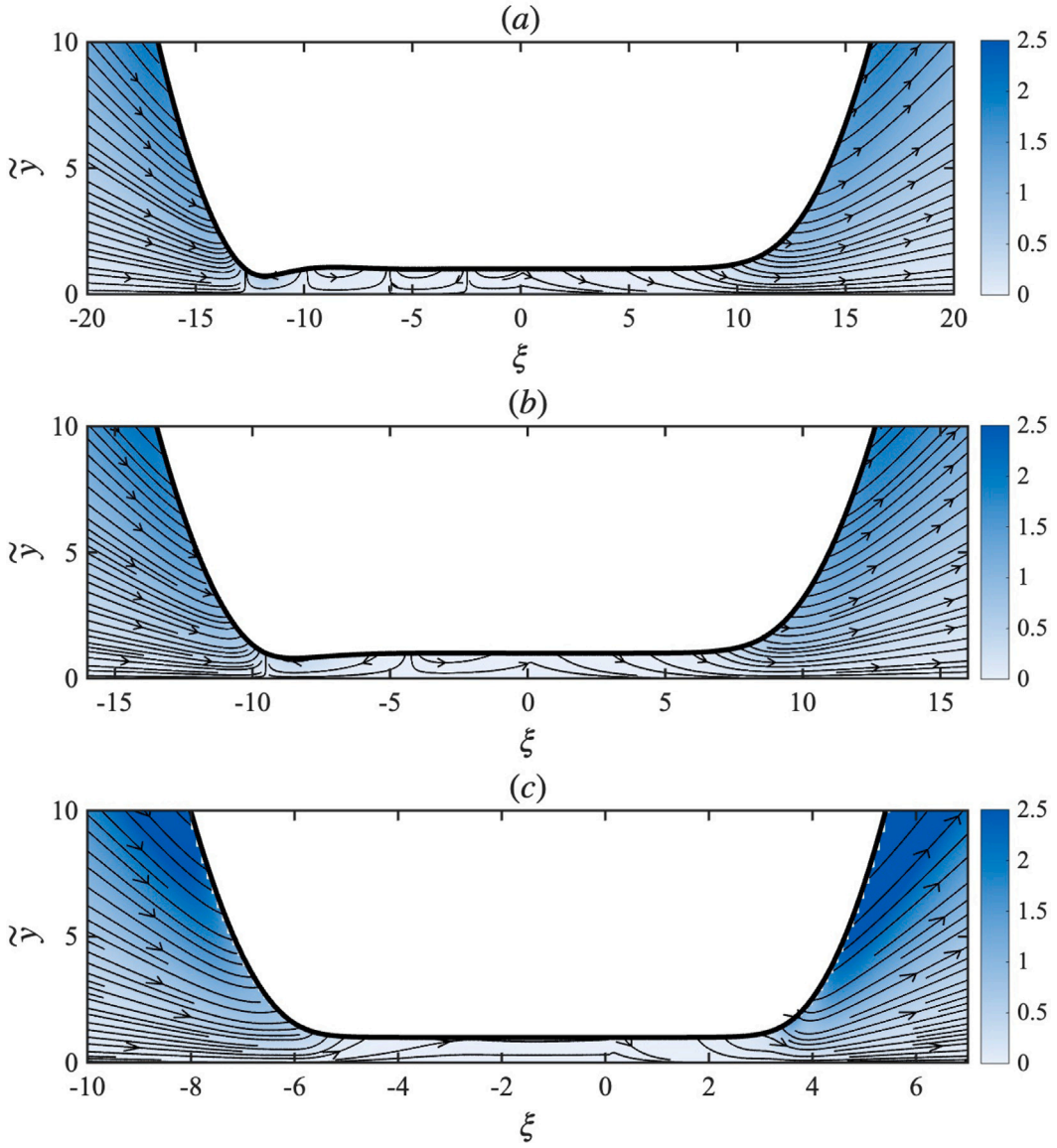

Fig. 3. Effect of the van der Waals parameter on the streamlines computed in the absolute reference frame in the thin film region of an elongated bubble in the Newtonian limit, $El \to \infty$ and $\alpha = 2$; (a) $\tilde{\beta} = 0$, (b) $\tilde{\beta} = 1$, (c) $\tilde{\beta} = 10$. The contours shows the magnitude of the velocity field $\sqrt{\tilde{u}^2 + \tilde{v}^2}$ in the absolute reference frame.

$$+(B - C)\sinh\left(\frac{\lambda_2 - \lambda_3}{2}\xi\right)\Bigg], \tag{25}$$

where the constant $B = 10^{-3}$ has the only effect of shifting the origin while C shifts the meniscus up or down. Interestingly, the undulations typical of the rear of the Bretherton bubble disappear from the approximated solution due to the stabilizing effect of the long-range van der Waals forces. Although it seems reasonable to apply the same iterative procedure described above to tune the constant C with the goal of matching the curvature of the rear with the one in the front, such procedure is not successful in this case. In the absence of experimental evidences of that for regimes dominated by the disjoining pressure we just set $C = B$. This suggests that, when the disjoining pressure is dominant for $\tilde{\beta} > 1.89$, the bubble shape in the rear is profoundly different compared t to the case with $\tilde{\beta} = 0$.

To sum up, the film equation Eq. (17) is integrated numerically starting from the approximated solution, which varies depending on the van der Waals parameter. The rear and the front are obtained separately and, then, artificially merged to provide the description of the whole thin-film region shown in Fig. 1.

3. Results and discussion

3.1. Shape of the elongated bubble

In this section, we investigate how the disjoining pressure affects the shape of the elongated bubble. To better visualize such effect on the film we solved the film equation for the rear and the front separately and, then, we merged them artificially. Doing so, the volume and the length of the bubble are arbitrary and can be set adjusting the integration constants introduced in Section 2.3. We will show the effect that intermolecular forces have on an elongated bubble with a fixed volume in Section 3.3.

In Fig. 2(a) we show the impact of the van der Waals parameter $\tilde{\beta}$ on the meniscus in the Newtonian limit where the shear-thinning effect is negligible, namely $El \to \infty$; note that this phenomenon is still unexplored in previous works on Newtonian films [see e.g., 48,49]. The disjoining pressure stabilizes the film, suppressing the undulations in the rear and steepening the profile as $\xi \to \infty$. Specifically, when the van der Waals forces are absent, the pressure evolution is only affected

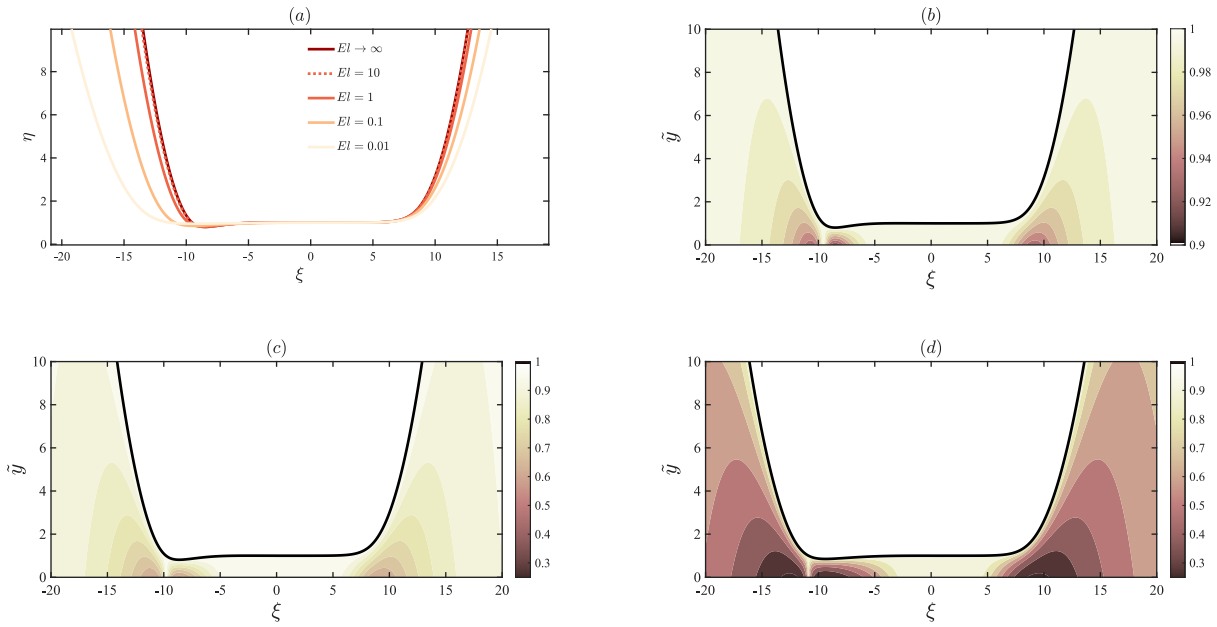

Fig. 4. (a) Effect of the Ellis number, El, on the shape of the meniscus for a shear thinning fluid with $\alpha = 2$ in the van der Waals regime, $\tilde{\beta} = 1$. (b) Contours of the effective viscosity for $El = 10$, $\alpha = 2$, and $\tilde{\beta} = 1$. (c) Contours of the effective viscosity for $El = 1$, $\alpha = 2$, and $\tilde{\beta} = 1$. (d) Contours of the effective viscosity for $El = 0.1$, $\alpha = 2$, and $\tilde{\beta} = 1$.

by the surface tension term via the interface curvature according to Eq. (12) as shown in Fig. 2(b). This contribution is constant when $\eta \gg 1$ and becomes negligible within the uniform film where the driving force vanishes: $d\bar{p}/d\xi = d^3\eta/d\xi^3 \approx 0$. In the rear, instead, due to the undulations of the meniscus, the driving force locally changes sign indicating the presence of recirculating vortexes, as shown Fig. 3(a). The streamlines have been obtained using the velocity profiles given in Appendix A with respect to the absolute reference frame.

As the van der Waals parameter increases, see Fig. 2(c), the contribution of the disjoining pressure becomes significant and it is maximum where the film thickness is minimum while, far from the uniform film, it decreases with $\sim \eta^{-3}$. In this case, the undulations are still present since $\tilde{\beta} < 1.89$ as shown in Fig. 3(b). However, when the van der Waals parameter is sufficiently high, the stabilizing effect of the disjoining pressure suppresses the undulations and the pressure profile is monotonic, see Fig. 2(d). The effect of the curvature is maximal (with respect to the disjoining pressure) in the front and the rear while negligible in the uniform film, and vice versa. As a result, although the curvatures of the front and rear are different as discussed in Section 2.3, the velocity field is qualitatively similar, see Fig. 3(c). This is a specific characteristic of the elongated bubble with $\tilde{\beta} > 1.89$.

The effect of the fluid rheology is shown in Fig. 4(a) for an elongated bubble in the van der Waals regime with $\tilde{\beta} = 1$. The shear-thinning effect reduces the steepness of meniscus in a similar way to that observed by Picchi et al. [38] in the absence of disjoining pressure. In fact, as shown above, the disjoining pressure is important only in the proximity of the uniform film, while in the front and rear the flow field is dominated by capillarity. The evolution of the pressure is similar to the Newtonian limit (not shown).

Interestingly, although the liquid behaves like a shear-thinning fluid, the flow is dominated by the zero-shear-rate effect in the uniform film ($\eta \approx 1$ and $\mu/\mu_0 \approx 1$), as shown by the effective viscosity contour in Fig. 4(b)–(c). The effective viscosity is calculated using Eqs. (6) and (7) in the limit of small capillary numbers (i.e., $\varepsilon \ll 1$) obtaining that the effective shear-rate is simply $|\partial\tilde{u}/\partial\tilde{y}|$. This feature of the uniform film is in line with the observations of recent works that have shown that, although the fluid exhibits a shear-thinning rheology, there may exist conditions where the flow field is indeed dominated by the zero-shear rate effects [see e.g., 26,27,30,38,40].

3.2. Scaling law for the film thickness

In this section, we discuss how the disjoining pressure and the fluid rheology affect the scaling law for the film thickness. As in the seminal work of Bretherton [10], since the meniscus in the front is spherical for $Ca \ll 1$, we can match it with the profile obtained from the film model. Specifically, far from the uniform film, the film model Eq. (17) can be simplified dividing both members for $\eta^{\alpha-1}$ and taking the limit of $\eta \gg 1$ to obtain an approximated equation where the terms accounting for the disjoining pressure ($\sim \eta^{-4}$) vanish

$$\frac{d^3\eta}{d\xi^3} \approx 0 \qquad \text{when} \quad \eta \gg 1\,, \tag{26}$$

and whose integration yields a parabolic profile

$$\eta = \frac{P}{2}\xi^2 + W\xi + Z, \tag{27}$$

where P, W, and Z are integration constants. Far from the uniform film, in fact, the dimensionless curvature given by $P = d^2\eta/d\xi^2$ assumes a constant value. Thus, we can match the curvature in the parabolic region written in terms of dimensional variables

$$\frac{d^2h}{dx^2} = \frac{(3Ca)^{2/3}}{h_\infty} P(\tilde{\beta}, El, \alpha), \tag{28}$$

with the curvature of the spherical cap $d^2h/dx^2 = 1/R$ obtaining the following scaling law

$$\frac{h_\infty}{R} = (3Ca)^{2/3} P(\tilde{\beta}, El, \alpha)\,. \tag{29}$$

This relation shows that the ratio between the uniform film thickness and the tube half width R is a function of the capillary number, the rescaled van der Waals parameter, the Ellis number, and the shear-thinning index only. The parameter P is obtained from the numerical solution of the film model discussed in Section 2.3. When the disjoining pressure is negligible for $\tilde{\beta} \to 0$ and the zero-shear-rate effect dominates over the shear-thinning effect for $El \to \infty$, we recover the same 2/3

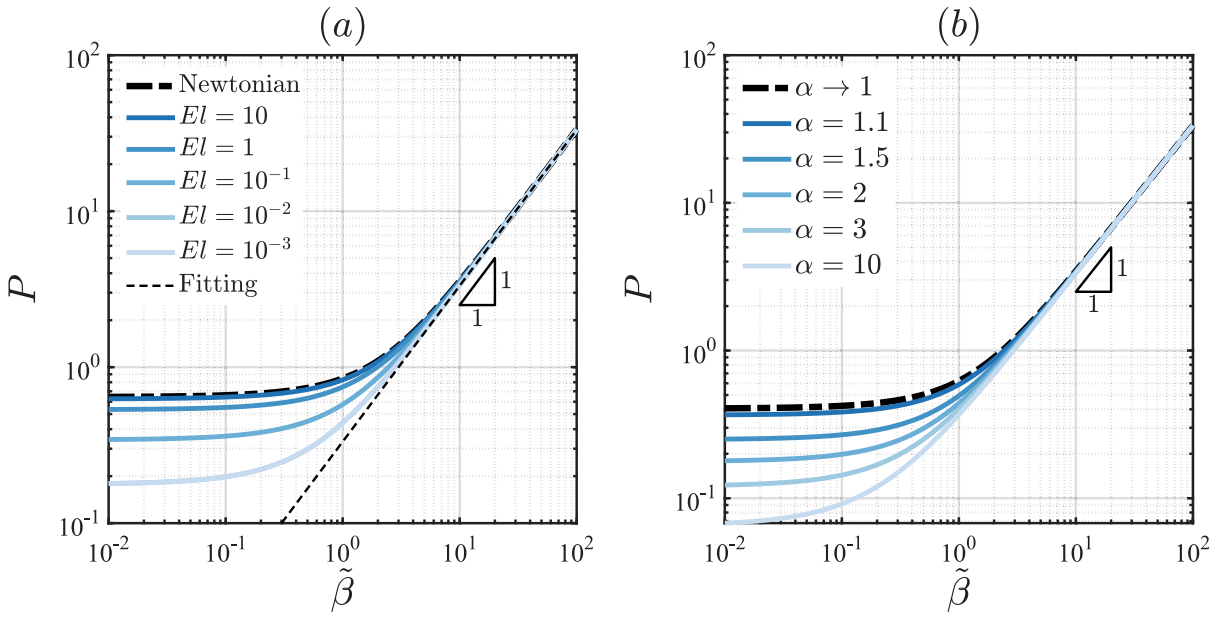

Fig. 5. (a) Evolution of the constant P with respect to the rescaled van der Waals parameter $\tilde{\beta}$ and the Ellis number El; $\alpha = 2$. The dashed line is the fitted curve for $\tilde{\beta} \gg 1$ (b) (a) Evolution of the constant P with respect to the rescaled van der Waals parameter $\tilde{\beta}$ and the shear thinning index α; in this case $El = 0.1$.

scaling law by Bretherton [10], namely $h_\infty/R = 0.643(3Ca)^{\frac{2}{3}}$. When $\tilde{\beta} \to 0$ but the shear thinning effect competes with surface tension, Eq. (29) reduces to the one discussed in Picchi et al. [38], namely $h_\infty/R = (3\mathrm{Ca})^{2/3} P(\tilde{\beta} \to 0, El, \alpha)$.

Since our interest is in showing how the van der-Waals forces affect the scaling law for the film thickness, Fig. 5(a) shows the evolution of P as a function of $\tilde{\beta}$ and El. When $\tilde{\beta} \to 0$ the curves approach a constant value equal to 0.643 in the Newtonian limit or a slightly lower value for decreasing value of El. This is a regime dominated by surface tension. When $\tilde{\beta} \gg 1$, instead, the curves collapse over the same master curve and lose the dependence on the Ellis number (i.e., El affects the scaling law only up to $\tilde{\beta} = \mathcal{O}(1)$). In this limit, P scales linearly with $\tilde{\beta}$ as $P \sim f(\alpha)\tilde{\beta}$ where $f(\alpha)$ is a function of the degree of shear thinning only; for $\alpha = 2$ we get by fitting $f = 0.693^3$. This is a regime dominated by the disjoining pressure where the shape of the bubble and the flow field are profoundly different compared to the limit of $\tilde{\beta} \to 0$ and the rheology has only a limited effect, see Fig. 3. The overall behavior is the same if we change the shear-thinning index α as shown in Fig. 5(b).

We can identify two different regimes: one at low $\tilde{\beta}$ dominated by capillarity (Bretherton regime) and one at high $\tilde{\beta}$ dominated by the disjoining pressure (van der Waals regime); the two are matched by a transition region. Since the Waals parameter is a function of Ca, the dependence of the film thickness on the capillary number is not explicit and it is worth recasting Eq. (29) introducing the dimensionless parameter

$$\ell = \left(\frac{A}{6\pi\sigma R^2}\right)^{1/2} = \frac{\ell_m}{R}, \tag{30}$$

that can be interpreted as the ratio of the molecular length scale, $\ell_m = \sqrt{A/(6\pi\sigma)}$, to the macroscopic length scale, R, and it typically assumes values in the range of 10^{-7}-10^{-3} (see [50]). Thus, the rescaled van der Waals parameter given in Eq. (18) can be written as

$$\tilde{\beta} = \frac{\ell^2}{(h_\infty/R)^2(3Ca)^{2/3}}. \tag{31}$$

Following the same procedure given in Hammoud et al. [50], combining Eqs. (31) e (29) we obtain two expressions that relate the film thickness (rescaled to a factor $\ell^{-2/3}$) and the capillary number (rescaled to a factor ℓ^{-1}) as

$$\ell^{-1}Ca = \frac{1}{3P(\tilde{\beta}, El, \alpha)\tilde{\beta}^{1/2}} \qquad \ell^{-\frac{2}{3}}\left(\frac{h}{R}\right) = \left(\frac{P(\tilde{\beta}, El, \alpha)}{\tilde{\beta}}\right)^{\frac{1}{3}}. \tag{32}$$

In Fig. 6(a) we show the evolution of the film thickness with respect to the capillary number as a function of the Ellis number. In the Bretherton regime ($\ell \ll Ca \ll 1$ and $\tilde{\beta} \ll 1$) the constant $P(El, \alpha)$ is a function of the fluid rheology only and Eq. (29) reduces to the same scaling law obtained by Picchi et al. [38]. Instead, in the van der Waals regime ($Ca \leq \mathcal{O}(\ell)$ and $\tilde{\beta} \gg 1$), since $P \sim f(\alpha)\tilde{\beta}$ (see Fig. 5), Eq. (32) can be simplified obtaining a constant film thickness that depends only on the shear-thinning index

$$\frac{h_\infty}{R} = f(\alpha)\,\ell^{\frac{2}{3}}. \tag{33}$$

The curves of Fig. 6(a) are still based on the capillary number based on the zero-shear-rate viscosity that may be not the relevant scale for viscosity when the shear-thinning effect is important. Interestingly, those curves can be collapsed over the same master curve introducing the effective capillary number similarly to what done in Picchi et al. [38]

$$Ca_e = \frac{\mu_e U}{\sigma} \quad \text{with} \quad \mu_e = \mu_0\left(\frac{P(\tilde{\beta} \to 0, El, \alpha)}{0.643}\right)^{\frac{3}{2}}. \tag{34}$$

The idea is to rescale the viscosity using the constant P in the limit of $\tilde{\beta} \to 0$. Combining (32) and (34) we get the generalized expressions that relates the film thickness (rescaled to a factor $\ell^{-2/3}$) and the effective capillary number (rescaled to a factor ℓ^{-1}) as

$$\ell^{-1}Ca_e = \frac{1}{3\tilde{\beta}^{1/2}\left(\frac{0.643P(\tilde{\beta}, El, \alpha)^{2/3}}{P(\tilde{\beta} \to 0, El, \alpha)}\right)^{\frac{3}{2}}} \qquad \ell^{-\frac{2}{3}}\left(\frac{h}{R}\right) = \left(\frac{P(\tilde{\beta}, El, \alpha)}{\tilde{\beta}}\right)^{\frac{1}{3}}. \tag{35}$$

These expressions allow us to collapse all the curves on the Newtonian one and generalize the scaling for the film thickness capturing both the Bretherton and the van der Waals regimes, see Fig. 6(b). The proposed master curve holds for both Newtonian and inelastic shear-thinning fluids and it is in agreement with previous results obtained for Newtonian fluids where, at ultra-low capillary numbers, the film

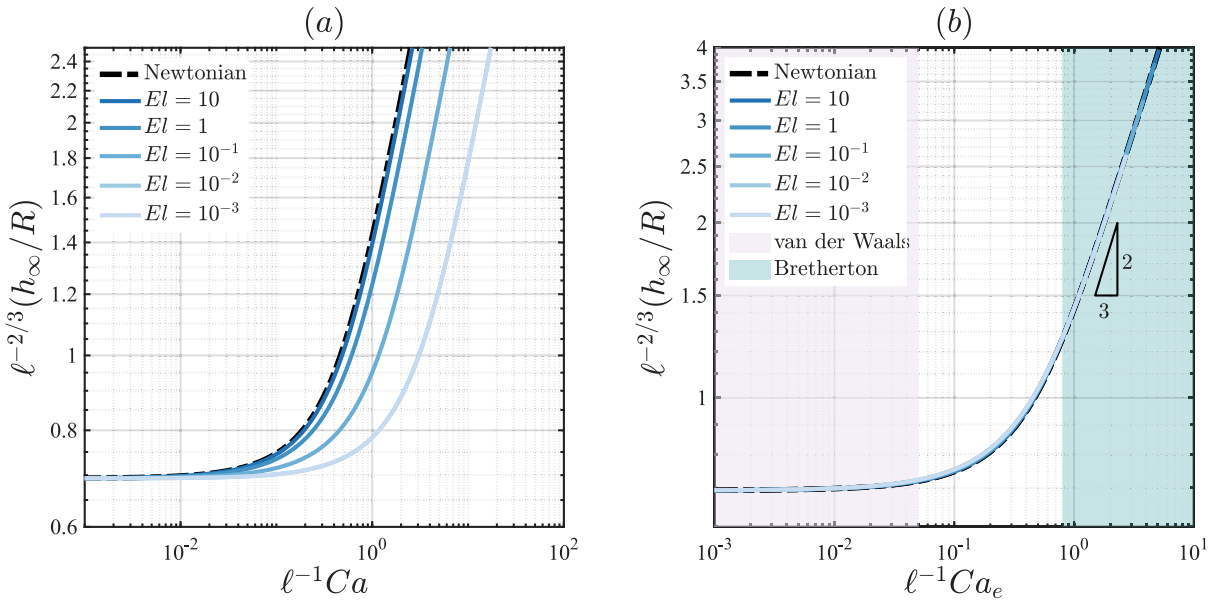

Fig. 6. (a) Evolution of the film thickness (rescaled to a factor $\ell^{-2/3}$) with respect to the capillary number (rescaled to a factor ℓ^{-1}) as a function of the Ellis number El; $\alpha = 2$. (b) Master curve for the film thickness (rescaled to a factor $\ell^{-2/3}$) with respect to the effective capillary number (rescaled to a factor ℓ^{-1}) with $\alpha = 2$.

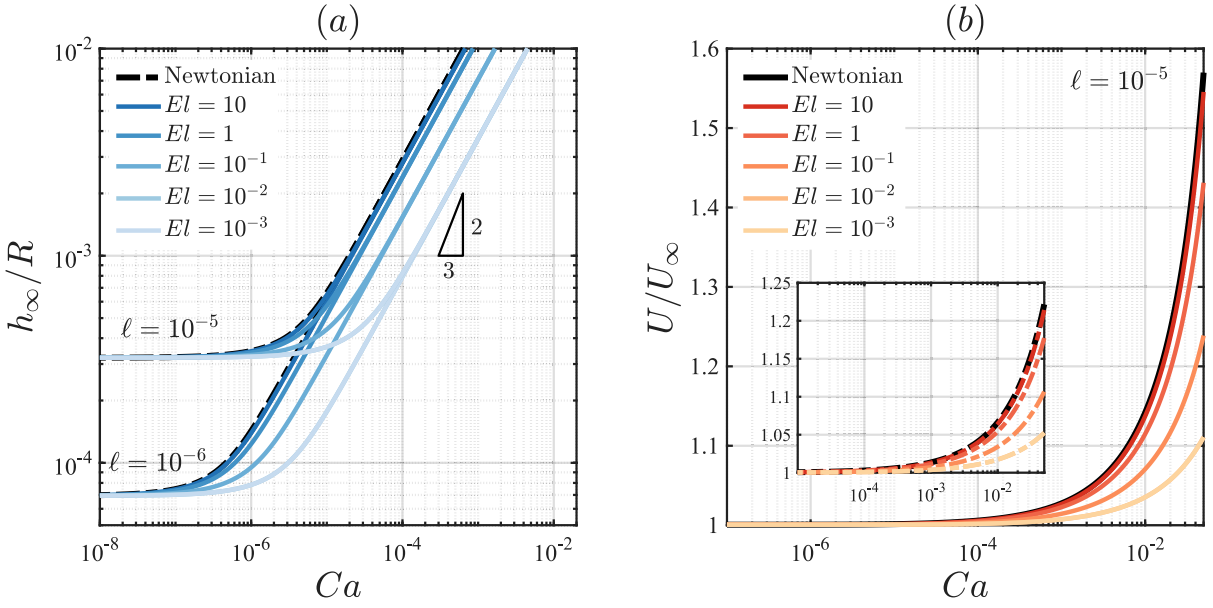

Fig. 7. (a) Evolution of the film thickness with respect to the capillary number as a function of the Ellis number El and the molecular length ratio ℓ; $\alpha = 2$. (b) Evolution of the speed ratio with respect to the capillary number as a function of the Ellis number El for $\ell = 10^{-5}$ and $\alpha = 2$ in a circular tube; the inset shows the speed ratio for a planar geometry.

thickness deviates from the Bretherton 2/3 scaling law and flattens to a constant value [48]. The observation that, despite the fluid being shear-thinning, the same scaling law as in the corresponding Newtonian case remains valid after an appropriate rescaling of the viscosity appears to be not just accidental, but rather a recurring characteristic across many different problems [see for example 31,38,40,41,55].

3.3. Ramifications for elongated bubble in channels and capillary tubes

In this section we explore the ramifications of our theory in terms of predicted film thickness and bubble speed as a function of the capillary number and the rheological parameters of the shear-thinning fluid.

Thanks to the scaling analysis of the previous section, we can conclude that the dimensionless film thickness is a function of the capillary number, the Ellis number, the shear-thinning index, and the molecular length ratio only as $h_\infty/R = h_\infty/R(Ca, El, \alpha, \ell)$. Among these dimensionless parameters, El, α, and ℓ can be determined *a priori* once the geometry and the fluid properties are known, while the capillary number depends on the bubble speed and, therefore, can be interpreted as the controlling parameter in real experiments adjusting the flow rate of the liquid far behind the bubble. In practical scenarios, the parameter ℓ typically assumes values in the range of 10^{-7}-10^{-3} given that the Hamaker constant A is in the range 10^{-20}–10^{-19} J, the surface tension σ is of the order of 10^{-2} J/m^2, and R is in of the order of $1 - 10^3$

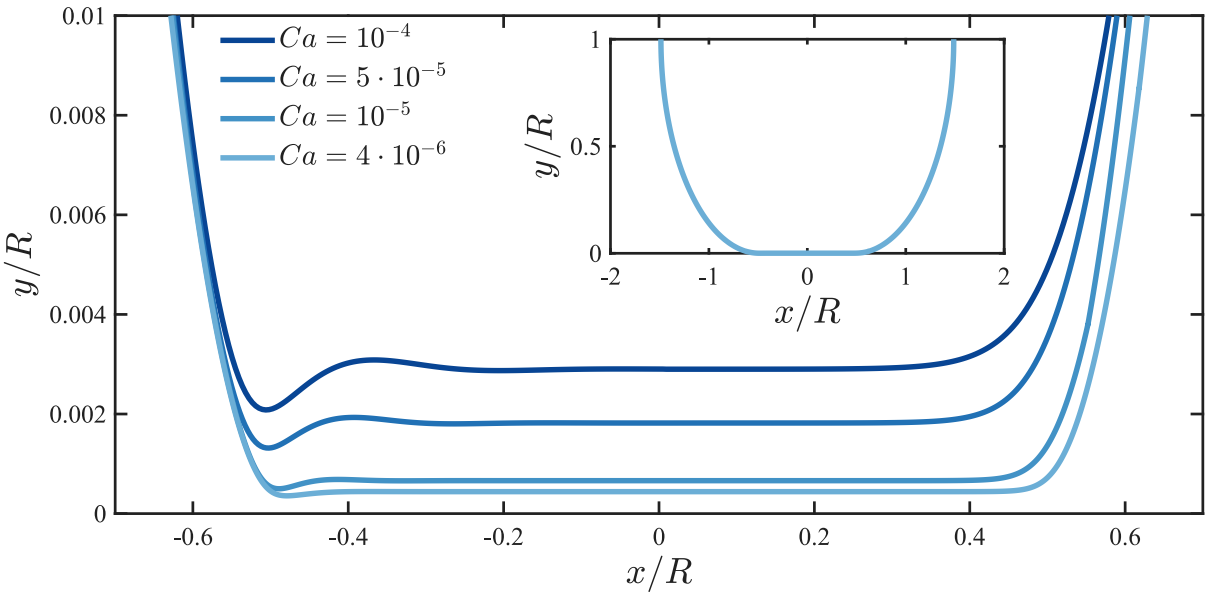

Fig. 8. Effect of the capillary number on the shape of the elongated bubble of fixed volume for $\ell = 10^{-5}$, $El = 10^{6}$, $\alpha = 2$. The inset shows the full channel, while the plot is a zoom of the film region in terms of spatial variables normalized to the tube radius.

μm [48,50,56]. In Fig. 7(a) we show the evolution of the film thickness for a shear-thinning fluid with respect to the capillary number for different value of the Ellis number and the molecular length ratio. This trends hold for both the planar and the circular geometries as shown in Section 2.1. Interestingly, decreasing ℓ (namely, increasing the gap between the molecular, ℓ_m, and the macroscopic, R, length scales) extends the Bretherton regime to lower Ca and lowers the plateau of the film thickness at ultra-low Ca. It is worth observing that, in the Van der Waals regime, the flow in the film is dominated by intermolecular forces and the effect of the rheology becomes negligible while, in the Bretherton regime the intermolecular effects becomes negligible and $h_\infty/R \sim Ca^{2/3}$.

The fact that at ultra-low capillary number the effect of the rheology vanishes agrees with the work by Neogi and Ybarra [57] on the spreading of the contact line for inelastic shear-thinning drops. Their main conclusion is that the spreading rates of thin-films are independent of the non-Newtonian nature of the fluids and, to a good approximation, the zero-shear-rate viscosity dominates such thin-films dynamics. This seems to be confirmed by our theoretical analysis, even though it is worth acknowledging its main limitations. In particular, we are assuming the fluid to be an inelastic shear-thinning fluid which results to be a good model only for polymer solutions under certain conditions (e.g., semi-rigid xhantane gum solutions). In fact, due to the finite size of such polymeric molecules, we are implicitly assuming that the continuum model and the Ellis viscosity model still hold at spatial scales comparable to the liquid film given by Eq. (33), namely of the order of $\mathcal{O}(R\ell^{\frac{2}{3}})$.

In Fig. 8 we show the effect of the capillary number on the bubble shape for an elongated bubble of fixed volume (the volume can be tuned via the integration constants introduced in Section 2.3). The bubble profile is obtained matching the thin film solution to the circular cap at the ends and it is plotted in terms of the spatial variables normalized with respect to the channel radius instead of the similarity variables used in previous sections. At such low capillary numbers the film is so thin that a magnification to the film region is need to appreciate the changes on the bubble shape; the profiles are almost undistinguishable if the whole tube is displayed, see the inset of Fig. 8. Specifically, as Ca decreases the uniform film become thinner and the undulations in the rear flattens due to the stabilizing effect of the disjoining pressure. As expected, since the film thins, the bubble becomes slightly longer; these variations of the bubble shape can be observed until the uniform film reaches its asymptotic value for $Ca \to 0$ and the stabilizing intermolecular forces becomes so strong that the bubble shape does not change anymore, see Fig. 7(a).

Once the scaling relation between the film thickness and the capillary number is known, it is straightforward to show that the bubble always flow faster than the fluid ahead, namely that $U/U_\infty > 1$. In fact, writing a mass balance between the uniform film region and the fluid ahead in a reference frame that moves with the bubble for a planar geometry

$$(0 - U)h_\infty = (U_\infty - U)R, \tag{36}$$

gives the relation between the speed ratio and the film thickness as

$$\frac{U}{U_\infty} = \frac{1}{1 - h_\infty/R}. \tag{37}$$

For a circular tube, the mass balance becomes

$$(0 - U)\pi\left(R^2 - (R - h_\infty)^2\right) = (U_\infty - U)\pi R^2, \tag{38}$$

and, in the limit of $h_\infty/R \ll 1$, reduces to

$$\frac{U}{U_\infty} = \frac{1}{1 - 2(h_\infty/R)}. \tag{39}$$

In Fig. 7(b) we show the evolution of the speed ratio as a function of the capillary number for both the circular and the planar (inset) geometries. In the Van der Waals regime (at ultra-low Ca) the speed ratio is close to the unity and the bubble is just slightly faster compared to the imposed volume flux. Similarly to what observed for the film thickness, the effect of the rheology is important only from capillary numbers where the transition region between the van der Waals and the Bretherton regimes takes place. Overall, the bubble always flows faster in a tube compared to the planar geometry in the whole range of capillary numbers.

4. Conclusions

In this work we studied an elongated bubble that moves through a shear-thinning fluid in regimes where the long-range van der Waals forces are important. In particular, we generalized the classical thin film model proposed by Bretherton [10] and later extended to shear-thinning fluids by Picchi et al. [38] to account for the effect of the

disjoining pressure. Specifically, we focused on regimes where the van der Waals forces are repulsive and, then, stabilize the thin film. In fact, the disjoining pressure dominates over capillarity near the uniform film region in the central part of the bubble while its effect is negligible near the spherical caps at the front and the rear of the bubble.

The main result of this work is a generalization of the scaling law for the film thickness with respect to the tube width that applies both to Newtonian and non-Newtonian fluids and captures either the van der Waals (at ultra-low capillary numbers where the intermolecular forces are dominant) and the Bretherton (at low capillary numbers where surface tension dominates over viscous effects and inertia) regimes. This has been done by a proper rescaling of the effective viscosity allowing us define a generalized capillary number. Interestingly, the effect of the rheology is more evident in the Bretherton regime, while, in the van der Waals regime, the film model predicts a constant value of the film thickness. We also believe that the proposed generalization of the thin-film equation for shear-thinning fluids to regimes where the stabilizing intermolecular forces are important could be a first step in the direction of describing also destabilizing effects or electrostatic effects.

CRediT authorship contribution statement

Davide Picchi: Writing – review & editing, Writing – original draft, Supervision, Funding acquisition, Formal analysis, Conceptualization. **Mohamed Berkani:** Software, Formal analysis. **Gianluca Lavalle:** Writing – review & editing, Supervision, Funding acquisition, Conceptualization. **Pietro Poesio:** Writing – review & editing, Supervision, Conceptualization.

Declaration of competing interest

The authors declare that they have no known competing financial interests or personal relationships that could have appeared to influence the work reported in this paper.

Acknowledgments

This work was supported by the Auvergne-Rhône-Alpes region through the project "MuscaFlow" (21 007147) agreed between Mines Saint-Etienne and Università degli Studi di Brescia.

Appendix A. Velocity profiles in the thin film

The x-component of the velocity profile $\tilde{u}$ is given in Eq. (14). In order to include the pre-factor 3 into the definition of the van der Waals parameter (the rescaled one given in Eq. (18)), namely

$$\frac{dp}{d\xi} = -\frac{d^3\eta}{d\xi^3} + \tilde{\beta}\frac{d\eta}{d\xi}\frac{1}{\eta^4}, \tag{A.1}$$

we rescale $\tilde{x} \to \xi$ and $\tilde{p} \to p$ obtaining

$$\tilde{u}(\tilde{y},\xi) = \frac{3}{2}\frac{dp}{d\xi}\left(\tilde{y}^2 - 2\eta\tilde{y}\right) + \frac{3^\alpha}{(\alpha+1)El^{\alpha-1}}\frac{dp}{d\xi}\left|\frac{dp}{d\xi}\right|^{\alpha-1}\left[(\eta-\tilde{y})^{\alpha+1} - \eta^{\alpha+1}\right]. \tag{A.2}$$

Using the continuity equation and integrating it over the film we get the transverse component of the velocity $\tilde{v}$ as

$$\tilde{v}(\xi,\tilde{y}) = -\int_0^{\tilde{y}} \frac{\partial\tilde{u}}{\partial\xi}\, d\tilde{y} \tag{A.3}$$

Accounting for the fact that the pressure gradient $dp/d\xi$ can be either positive or negative, the velocity components can be written as

$$\tilde{u}(\tilde{y},\xi) = \frac{3}{2}\frac{dp}{d\xi}\left(\tilde{y}^2 - 2\eta\tilde{y}\right) + \mathrm{sgn}\left(\frac{dp}{d\xi}\right)\frac{3^\alpha}{(\alpha+1)El^{\alpha-1}}\left|\frac{dp}{d\xi}\right|^{\alpha}\left[(\eta-\tilde{y})^{\alpha+1} - \eta^{\alpha+1}\right] \tag{A.4}$$

and

$$\tilde{v}(\xi,\tilde{y}) = -\frac{3}{2}\frac{d^2p}{d\xi^2}\left(\frac{\tilde{y}^3}{3} - \eta\tilde{y}^2\right) + 3\frac{dp}{d\xi}\frac{d\eta}{d\xi}\frac{\tilde{y}^2}{2} + \\ + \frac{3^\alpha}{(\alpha+1)El^{\alpha-1}}\left\{\alpha\left|\frac{dp}{d\xi}\right|^{\alpha-1}\frac{d^2p}{d\xi^2}\left(\frac{(\eta-\tilde{y})^{\alpha+2} - \eta^{\alpha+2}}{\alpha+2} + \tilde{y}\eta^{\alpha+1}\right) + \right. \\ \left. + \mathrm{sgn}\left(\frac{dp}{d\xi}\right)(\alpha+1)\left|\frac{dp}{d\xi}\right|^{\alpha}\frac{d\eta}{d\xi}\left(\frac{(\eta-\tilde{y})^{\alpha+1} - \eta^{\alpha+1}}{\alpha+1} + \tilde{y}\eta^{\alpha}\right)\right\}, \tag{A.5}$$

where

$$\frac{d^2p}{d\xi^2} = -\frac{d^4\eta}{d\xi^4} + \tilde{\beta}\frac{d^2\eta}{d\xi^2}\frac{1}{\eta^4} - 4\tilde{\beta}\left(\frac{d\eta}{d\xi}\right)^2\frac{1}{\eta^5}. \tag{A.6}$$

Appendix B. Analysis of the film equation near the uniform film

In this section we show that neglecting the shear-thinning term of the film model, Eq. (17), or its linearization near the uniform film, Eq. (19), is consistent. In Fig. B.9(a) we show the evolution of the three terms of the film model Eq. (17) for $\tilde{\beta} = 1$, $El = 0.01$, and $\alpha = 2$, namely

$$T_1 = \frac{d^3\eta}{d\xi^3} - \frac{\tilde{\beta}}{\eta^4}\frac{d\eta}{d\xi}, \tag{B.1}$$

$$T_2 = \frac{3^\alpha}{(\alpha+2)El^{\alpha-1}}\left(\frac{d^3\eta}{d\xi^3} - \frac{\tilde{\beta}}{\eta^4}\frac{d\eta}{d\xi}\right)\left|-\frac{d^3\eta}{d\xi^3} + \frac{\tilde{\beta}}{\eta^4}\frac{d\eta}{d\xi}\right|^{\alpha-1}\eta^{\alpha-1}, \tag{B.2}$$

$$T_3 = \frac{\eta-1}{\eta^3}. \tag{B.3}$$

Near the origin where $\eta \approx 1$, we can observe that the second term (the one that account for the shear-thinning effect) becomes negligible compared to the other two. To demonstrate this we can recast Eq. (17) as

$$\left(\frac{d^3\eta}{d\xi^3} - \frac{\tilde{\beta}}{\eta^4}\frac{d\eta}{d\xi}\right)\left[1 + \underbrace{\frac{3^\alpha}{(\alpha+2)El^{\alpha-1}}\left|-\frac{d^3\eta}{d\xi^3} + \frac{\tilde{\beta}}{\eta^4}\frac{d\eta}{d\xi}\right|^{\alpha-1}\eta^{\alpha-1}}_{\ll 1}\right] = \frac{\eta-1}{\eta^3}, \tag{B.4}$$

and observing that, since both the first and the third derivative of η are small, the square parenthesis is just ≈ 1. The same arguments holds also for the linearized film equation Eq. (19) as shown in B.9(b).

With this we wanted to justify why in Section 2.3, we dropped the third term on the l.h.s. of Eq. (19) and the approximation near the uniform film is the same of the Newtonian problem.

Appendix C. Thin-film model for a power-law fluid

If we take the limit for $El \to 0$ from Eq. (17) the first two Newtonian terms can be dropped and we obtain the thin-film model for a power-law fluid whose viscosity is given by $\mu = \kappa\dot{\gamma}^{1/\alpha-1}$ with $\kappa = \mu_0^{1/\alpha}\tau_{1/2}^{(1-1/\alpha)}$. Specifically, Eq. (17) becomes

$$\frac{3^\alpha}{(\alpha+2)El^{\alpha-1}}\left(\frac{d^3\eta}{d\xi^3} - \frac{\tilde{\beta}}{\eta^4}\frac{d\eta}{d\xi}\right)\left|-\frac{d^3\eta}{d\xi^3} + \frac{\tilde{\beta}}{\eta^4}\frac{d\eta}{d\xi}\right|^{\alpha-1}\eta^{\alpha-1} = \frac{\eta-1}{\eta^3}, \tag{C.1}$$

where the sum of the capillary pressure and the disjoining pressure is the driving force in the film. Considering only cases where the driving force is positive, the argument of the absolute value is negative and the film model simplifies to

$$\frac{3}{(\alpha+2)^{\frac{1}{\alpha}}El^{\frac{\alpha-1}{\alpha}}}\left(\frac{d^3\eta}{d\xi^3} - \frac{\tilde{\beta}}{\eta^4}\frac{d\eta}{d\xi}\right) = \frac{(\eta-1)^{\frac{1}{\alpha}}}{\eta^{\frac{2+\alpha}{\alpha}}}. \tag{C.2}$$

Since the model is still written using the zero-shear-rate viscosity as the reference scale for viscosity, we can reparametrize Eq. (C.2) introducing

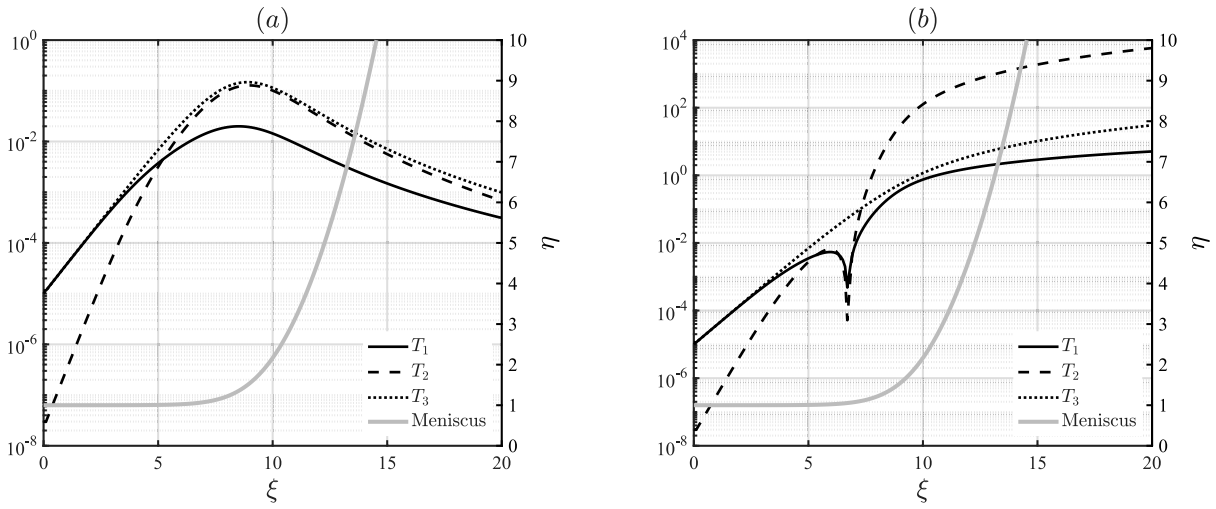

Fig. B.9. (a) Evolution of the three terms of the film model Eq. (17) for $\tilde{\beta} = 1$, $El = 0.01$, and $\alpha = 2$. (b) Evolution of the three terms of the linearized film model Eq. (19) for $\tilde{\beta} = 1$, $El = 0.01$, and $\alpha = 2$.

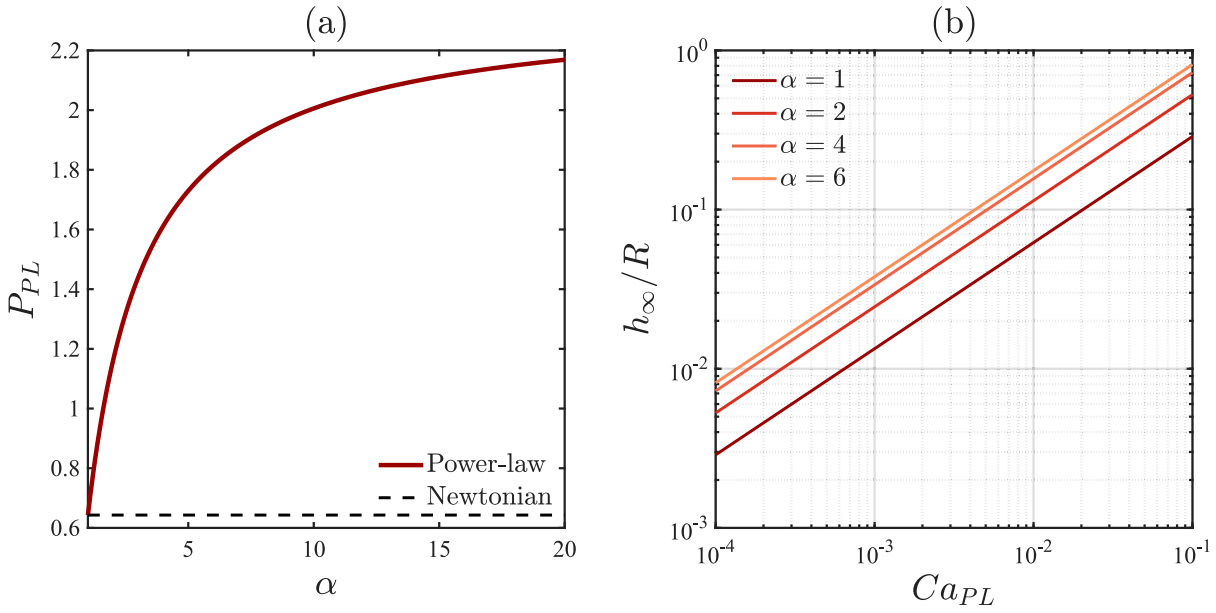

Fig. C.10. (a) Evolution of the dimensionless curvature as a function of the shear-thinning index for a power-law fluid; $\tilde{\beta}_{PL} = 0$. (b) Film thickness as a function of the capillary number for a power-law fluid with $\tilde{\beta}_{PL} = 0$.

a new length scale in the axial direction specific for the power-law fluid as

$$X = \frac{x}{h_\infty (3Ca_{PL})^{-\frac{1}{3}}} \qquad \text{with} \qquad Ca_{PL} = \frac{\mu_{PL} U}{\sigma}, \tag{C.3}$$

where Ca_{PL} is the capillary number reformulated using the viscosity scale for a power-law fluid

$$\mu_{PL} = \mu_0^{\frac{1}{\alpha}} \tau_{1/2}^{\frac{\alpha-1}{\alpha}} \left(\frac{U}{h_\infty}\right)^{\frac{1}{\alpha}-1} \frac{(\alpha+2)^{\frac{1}{\alpha}}}{3} = \kappa \left(\frac{U}{h_\infty}\right)^{\frac{1}{\alpha}-1} \frac{(\alpha+2)^{\frac{1}{\alpha}}}{3}. \tag{C.4}$$

The new capillary number is related to the one previously defined in Section 2.1 via the following expression

$$Ca_{PL} = CaEl^{\frac{\alpha-1}{\alpha}} \frac{(\alpha+2)^{\frac{1}{\alpha}}}{3}. \tag{C.5}$$

Thus, the film equation for a power-law fluid is given by

$$\frac{d^3\eta}{dX^3} - \frac{\tilde{\beta}_{PL}}{\eta^4}\frac{d\eta}{dX} = \frac{(\eta-1)^{\frac{1}{\alpha}}}{\eta^{\frac{2+\alpha}{\alpha}}}, \tag{C.6}$$

where $\tilde{\beta}_{PL}$ is the van der Waals parameter for a power-law fluid

$$\tilde{\beta}_{PL} = \frac{A}{2\pi h_\infty^2 \sigma (3Ca_{PL})^{\frac{2}{3}}}. \tag{C.7}$$

Note that Eq. (C.6) with $\tilde{\beta}_{PL} = 0$ is the same obtained by Kamişli and Ryan [18]. Eq. (C.6) can be solved numerically starting from a region where $\eta \approx 1$, $d\eta/dX \approx 0$, and $d^2\eta/dX^2 \approx 0$ using solver *ode45* od Matlab. Differently from the case of an Ellis fluid (see Section 2.3), the film equation for a power-law fluid do not admit an analytical solution near the uniform film and, therefore, the integration start has to be guessed. Far from the uniform film, instead, the behavior is quite similar to what obtained in Section 3.2 since for $\eta \gg 1$ Eq. (C.6) admits

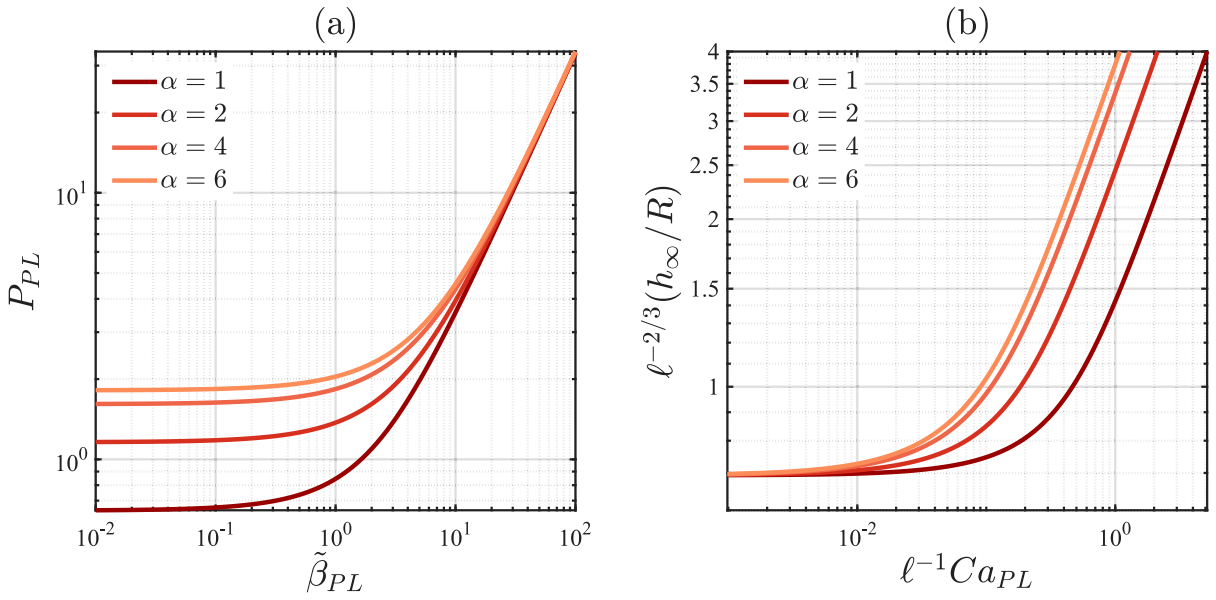

Fig. C.11. (a) Evolution of the dimensionless curvature as a function of the shear-thinning index and the van der Waals parameter for a power-law fluid. (b) Rescaled film thickness as a function of the capillary number for a power-law fluid and the shear-thinning index.

a parabolic solution of the type

$$\eta = \frac{P_{PL}}{2} X^2 + W_{PL} X + Z_{PL}. \tag{C.8}$$

The matching of the curvature between the film and the spherical cap yields to the following scaling law

$$\frac{h_\infty}{R} = (3Ca_{PL})^{2/3} P_{PL}(\alpha, \tilde{\beta}_{PL}). \tag{C.9}$$

In regimes where the van der Waals forces are negligible (i.e., $\tilde{\beta}_{PL} = 0$), the film thickness is uniquely a function of the shear-thinning index and the capillary number as shown in Fig. C.10. Note that for $\tilde{\beta}_{PL} = 0$, Eq. (C.9) is equivalent to Eq. (29) in the limit of $P(\tilde{\beta} = 0, El \to 0, \alpha)$ while replacing Ca with Ca_{PL} via Eq. (C.5).

In the van der Waal regime, the overall behavior is similar to what described in Section 3.2 and the film thickness saturates at ultra-low capillary number due to the stabilizing effect of the disjoining pressure as shown in Fig. C.11. Interestingly, the effect of the rheology is completely negligible for $Ca \to 0$.

Data availability

Data will be made available on request.

References

[1] V. Ajaev, G. Homsy, Modeling shapes and dynamics of confined bubbles, Annu. Rev. Fluid Mech. 38 (1) (2006) 277–307.

[2] R. Chhabra, Bubbles, Drops, and Particles in Non-Newtonian Fluids, CRC Press, 2007.

[3] A.S. Lynn, Droplets and bubbles in microfluidic devices, Annu. Rev. Fluid Mech. 48 (1) (2016) 285–309.

[4] S. Khodaparast, M.K. Kim, J.E. Silpe, H.A. Stone, Bubble-driven detachment of bacteria from confined microgeometries, Environ. Sci. Technol. 51 (3) (2017) 1340–1347.

[5] J. Grotberg, Pulmonary flow and transport phenomena, Annu. Rev. Fluid Mech. 26 (1) (1994) 529–571.

[6] J.L. Bull, Cardiovascular bubble dynamics, Crit. Rev. Biomed. Eng. 33 (4) (2005) 299–346.

[7] A. Suzuki, D.M. Eckman, Embolism bubble adhesion force in excised perfused microvessels, Anesthesiology 99 (2003) 400–408.

[8] D.M. Eckmann, V.N. Lomivorotov, Microvascular gas embolization clearance following perfluorocarbon administration, J. Appl. Physiol. 94 (3) (2003) 860–868.

[9] G. Taylor, Deposition of a viscous fluid on the wall of a tube, J. Fluid Mech. 10 (2) (1961) 161–165.

[10] F.P. Bretherton, The motion of long bubbles in tubes, J. Fluid Mech. 10 (2) (1961) 166–188.

[11] F. Fairbrother, A.E. Stubbs, 119. Studies in electro-endosmosis. Part VI. The "bubble-tube" method of measurement, J. Chem. Soc. (Resumed) (1935) 527–529.

[12] P. Aussillous, D. Quéré, Quick deposition of a fluid on the wall of a tube, Phys. Fluids 12 (10) (2000) 2367–2371.

[13] B. Cox, On driving a viscous fluid out of a tube, J. Fluid Mech. 14 (1) (1962) 81–96.

[14] M. Heil, Finite Reynolds number effects in the Bretherton problem, Phys. Fluids 13 (9) (2001) 2517–2521.

[15] S. Khodaparast, M. Magnini, N. Borhani, J.R. Thome, Dynamics of isolated confined air bubbles in liquid flows through circular microchannels: an experimental and numerical study, Microfluid. Nanofluidics 19 (1) (2015) 209–234.

[16] M. Magnini, A. Ferrari, J. Thome, H.A. Stone, Undulations on the surface of elongated bubbles in confined gas-liquid flows, Phys. Rev. Fluids 2 (8) (2017) 084001.

[17] Y.E. Yu, L. Zhu, S. Shim, J. Eggers, H.A. Stone, Time-dependent motion of a confined bubble in a tube: transition between two steady states, J. Fluid Mech. 857 (2018).

[18] F. Kamişli, M.E. Ryan, Perturbation method in gas-assisted power-law fluid displacement in a circular tube and a rectangular channel, Chem. Eng. J. 75 (3) (1999) 167–176.

[19] F. Kamişli, M.E. Ryan, Gas-assisted non-Newtonian fluid displacement in circular tubes and noncircular channels, Chem. Eng. Sci. 56 (16) (2001) 4913–4928.

[20] D.A. de Sousa, E.J. Soares, R.S. de Queiroz, R.L. Thompson, Numerical investigation on gas-displacement of a shear-thinning liquid and a visco-plastic material in capillary tubes, J. Non-Newton. Fluid Mech. 144 (2) (2007) 149–159.

[21] R.L. Thompson, E.J. Soares, R.D. Bacchi, Further remarks on numerical investigation on gas displacement of a shear-thinning liquid and a visco-plastic material in capillary tubes, J. Non-Newton. Fluid Mech. 165 (7) (2010) 448–452.

[22] A. Kawahara, M. Sadatomi, W.Z. Law, M.H. Mansour, Characteristics of gas and non-newtonian liquid two-phase flows through a circular microchannel, Multiph. Sci. Technol. 27 (2–4) (2015).

[23] M. Fatehifar, A. Revell, M. Jabbari, Non-Newtonian droplet generation in a cross-junction microfluidic channel, Polymers 13 (12) (2021).

[24] Q. Zhao, H. Ma, Y. Liu, C. Yao, L. Yang, G. Chen, Hydrodynamics and mass transfer of Taylor bubbles flowing in non-Newtonian fluids in a microchannel, Chem. Eng. Sci. 231 (2021) 116299.

[25] R. Bird, R. Armstrong, O. Hassager, Dynamics of Polymeric Liquids Vol 1: Fluid Mechanics, John Wiley and Sons Inc. United States, 1987.

[26] S. Shahsavari, G.H. McKinley, Mobility of power-law and Carreau fluids through fibrous media, Phys. Rev. E 92 (2015) 063012, http://dx.doi.org/10.1103/PhysRevE.92.063012.

[27] D. Picchi, P. Poesio, A. Ullmann, N. Brauner, Characteristics of stratified flows of Newtonian/non-Newtonian shear-thinning fluids, Int. J. Multiph. Flow 97 (2017) 109–133, http://dx.doi.org/10.1016/j.ijmultiphaseflow.2017.06.005.

[28] D. Picchi, A. Ullmann, N. Brauner, Modeling of core-annular and plug flows of Newtonian/non-Newtonian shear-thinning fluids in pipes and capillary tubes, Int. J. Multiph. Flow 103 (2018) 43–60, http://dx.doi.org/10.1016/j.ijmultiphaseflow.2018.01.023.
[29] D. Picchi, I. Barmak, A. Ullmann, N. Brauner, Stability of stratified two-phase channel flows of Newtonian/non-Newtonian shear-thinning fluids, Int. J. Multiph. Flow 99 (2018) 111–131, http://dx.doi.org/10.1016/j.ijmultiphaseflow.2017.10.001.
[30] E. Boyko, H.A. Stone, Flow rate2013pressure drop relation for shear-thinning fluids in narrow channels: approximate solutions and comparison with experiments, J. Fluid Mech. 923 (2021) R5, http://dx.doi.org/10.1017/jfm.2021.621.
[31] C. Steinik, D. Picchi, G. Lavalle, P. Poesio, Capillary imbibition of shear-thinning fluids: From Lucas-Washburn to oscillatory regimes, Phys. Rev. Fluids 9 (2024) 023305, http://dx.doi.org/10.1103/PhysRevFluids.9.023305.
[32] R. Hewson, N. Kapur, P. Gaskell, A model for film-forming with Newtonian and shear-thinning fluids, J. Non-Newton. Fluid Mech. 162 (1–3) (2009) 21–28.
[33] M. Reiner, Deformation, Strain, and Flow, Interscience, New York, 1965, p. 246.
[34] A.I. Moreira, L.A. Rocha, J. Carneiro, J.D. Araújo, J.B. Campos, J.M. Miranda, Isolated Taylor bubbles in co-current with shear thinning cmc solutions in microchannels—A numerical study, Processes 8 (2) (2020) 242.
[35] S.G. Sontti, A. Atta, CFD study on Taylor bubble characteristics in Carreau-Yasuda shear thinning liquids, Can. J. Chem. Eng. 97 (2) (2019) 616–624.
[36] P.J. Carreau, Rheological equations from molecular network theories, Trans. Soc. Rheol. 16 (1) (1972) 99–127.
[37] K. Yasuda, R. Armstrong, R. Cohen, Shear flow properties of concentrated solutions of linear and star branched polystyrenes, Rheol. Acta 20 (1981) 163–178, http://dx.doi.org/10.1007/BF01513059.
[38] D. Picchi, A. Ullmann, N. Brauner, P. Poesio, Motion of a confined bubble in a shear-thinning liquid, J. Fluid Mech. 918 (2021) http://dx.doi.org/10.1017/jfm.2021.321.
[39] H.A. Stone, Interfaces: in fluid mechanics and across disciplines, J. Fluid Mech. 645 (2010) 1–25, http://dx.doi.org/10.1017/S0022112009994186.
[40] A. Aquino, D. Picchi, P. Poesio, Dynamics of a Taylor bubble through a shear-thinning fluid up to finite capillary numbers, J. Non-Newton. Fluid Mech. 314 (2023) 105003, http://dx.doi.org/10.1016/j.jnnfm.2023.105003.
[41] S. Chun, B. Ji, Z. Yang, V.K. Malik, J. Feng, Experimental observation of a confined bubble moving in shear-thinning fluids, J. Fluid Mech. 953 (2022) A12, http://dx.doi.org/10.1017/jfm.2022.926.
[42] A. Oron, S.H. Davis, S.G. Bankoff, Long-scale evolution of thin liquid films, Rev. Modern Phys. 69 (1997) 931–980, http://dx.doi.org/10.1103/RevModPhys.69.931.
[43] L.G. Leal, Advanced transport phenomena: Fluid mechanics and convective transport processes, in: Cambridge Series in Chemical Engineering, Cambridge University Press, 2007.
[44] I. Dzyaloshinskii, E. Lifshitz, L. Pitaevskii, The general theory of van der Waals forces, Adv. Phys. 10 (38) (1961) 165–209, http://dx.doi.org/10.1080/00018736100101281.
[45] E. Lifshitz, M. Hamermesh, 26 - the theory of molecular attractive forces between solids reprinted from soviet physics JETP 2, Part 1, 73, 1956, in: L. Pitaevskii (Ed.), Perspectives in Theoretical Physics, Pergamon, Amsterdam, 1992, pp. 329–349, http://dx.doi.org/10.1016/B978-0-08-036364-6.50031-4.
[46] B. Dai, L.G. Leal, A. Redondo, Disjoining pressure for nonuniform thin films, Phys. Rev. E 78 (2008) 061602, http://dx.doi.org/10.1103/PhysRevE.78.061602.
[47] H. Chen, E. Dong, J. Li, H.A. Stone, Adhesion of moving droplets in microchannels, Appl. Phys. Lett. 103 (13) (2013) 131605, http://dx.doi.org/10.1063/1.4823456.
[48] K. Chaudhury, P.V. Acharya, S. Chakraborty, Influence of disjoining pressure on the dynamics of steadily moving long bubbles inside narrow cylindrical capillaries, Phys. Rev. E 89 (2014) 053002, http://dx.doi.org/10.1103/PhysRevE.89.053002.
[49] K. Chaudhury, S. Chakraborty, Scaling regimes of thermocapillarity-driven dynamics of confined long bubbles: Effects of disjoining pressure, Phys. Rev. E 91 (2015) 033021, http://dx.doi.org/10.1103/PhysRevE.91.033021.
[50] N.H. Hammoud, P.H. Trinh, P.D. Howell, H.A. Stone, Influence of van der Waals forces on a bubble moving in a tube, Phys. Rev. Fluids 2 (2017) 063601, http://dx.doi.org/10.1103/PhysRevFluids.2.063601.
[51] S. Matsuhisa, R.B. Bird, Analytical and numerical solutions for laminar flow of the non-Newtonian ellis fluid, AIChE J. 11 (4) (1965) 588–595.
[52] P.G. de Gennes, F. Brochard-Wyart, D. Quéré, Capillarity and Wetting Phenomena: Drops, Bubbles, Pearls, Waves, Springer, 2003.
[53] J. Eggers, M.A. Fontelos, Singularities: Formation, structure, and propagation, in: Cambridge Texts in Applied Mathematics, Cambridge University Press, 2015, http://dx.doi.org/10.1017/CBO9781316161692.
[54] B. Dai, L.G. Leal, A. Redondo, Disjoining pressure for nonuniform thin films, Phys. Rev. E 78 (2008) 061602, http://dx.doi.org/10.1103/PhysRevE.78.061602.
[55] I. Barmak, D. Picchi, A. Gelfgat, N. Brauner, Flow of a shear-thinning fluid in a rectangular duct, Phys. Rev. Fluids 9 (2024) 023303, http://dx.doi.org/10.1103/PhysRevFluids.9.023303, URL: https://link.aps.org/doi/10.1103/PhysRevFluids.9.023303.
[56] J.D. Chen, Measuring the film thickness surrounding a bubble inside a capillary, J. Colloid Interface Sci. 109 (2) (1986) 341–349, http://dx.doi.org/10.1016/0021-9797(86)90313-9, URL: https://www.sciencedirect.com/science/article/pii/0021979786903139.
[57] P. Neogi, R.M. Ybarra, The absence of a rheological effect on the spreading of small drops, J. Chem. Phys. 115 (17) (2001) 7811–7813, http://dx.doi.org/10.1063/1.1415455.